Adaptive Cancelation of Self-Generated Sensory Signals in a Whisking Robot

Sean R. Anderson, Martin J. Pearson, Anthony Pipe, Tony Prescott, Paul Dean, and John Porrill

***Abstract*—Sensory signals are often caused by one's own active movements. This raises a problem of discriminating between self-generated sensory signals and signals generated by the external world. Such discrimination is of general importance for robotic systems, where operational robustness is dependent on the correct interpretation of sensory signals. Here, we investigate this problem in the context of a whiskered robot. The whisker sensory signal comprises two components: one due to contact with an object (externally generated) and another due to active movement of the whisker (self-generated). We propose a solution to this discrimination problem based on adaptive noise cancelation, where the robot learns to predict the sensory consequences of its own movements using an adaptive filter. The filter inputs (copy of motor commands) are transformed by Laguerre functions instead of the often-used tapped-delay line, which reduces model order and, therefore, computational complexity. Results from a contact-detection task demonstrate that false positives are significantly reduced using the proposed scheme.**

***Index Terms*—Force and tactile sensing, internal model, learning and adaptive systems, neurorobotics, noise cancelation.**

I. Introduction

ACTIVE exploration of the environment is a necessary behavioral feature of both animals and mobile robots, for the purposes of navigation, object localization, and object recognition (see, e.g., [1]). However, active movements will often generate sensations in their own right, leading to a discrimination problem: What sensory signals are caused by one's own movements, and what sensory signals are caused by the external world? It is essential that an autonomous agent, either animal or robot, is able to make this distinction in order to interact with the environment in a robust manner. Falsely interpreting sensations could lead to catastrophic consequences for a robot, especially when dealing with threats or opportunities.

Manuscript received November 6, 2009; revised April 30, 2010; accepted August 11, 2010. Date of publication September 30, 2010; date of current version December 8, 2010. This work was supported by European Union under Grant Integrating Cognition, Emotion, and Autonomy IST-027819 and Grant Biomimetic Technology for Vibrissal Active Touch ICT-215910. This paper was recommended for publication by Associate Editor S. Hirai and Editor K. Lynch upon evaluation of the reviewers' comments.

S. R. Anderson is with the Department of Automatic Control and Systems Engineering, University of Sheffield, Sheffield S1 3JD, U.K. (e-mail: s.anderson@sheffield.ac.uk).

M. J. Pearson and A. Pipe are with the Bristol Robotics Laboratory, Bristol BS16 1QD, U.K. (e-mail: martin.pearson@brl.ac.uk; tony.pipe@brl.ac.uk).

T. Prescott is with the Active Touch Laboratory, University of Sheffield, Sheffield S10 2TP, U.K. (e-mail: t.j.prescott@sheffield.ac.uk).

P. Dean and J. Porrill are with the Department of Psychology, University of Sheffield, Sheffield S10 2TP, U.K. (e-mail: p.dean@sheffield.ac.uk; j.porrill@sheffield.ac.uk).

Color versions of one or more of the figures in this paper are available online at http://ieeexplore.ieee.org.

Digital Object Identifier 10.1109/TRO.2010.2069990

Recently, we have encountered an instance of this very problem in the operation of a whisking mobile robot, a prototype of which is described in [2] and [3]. Robotic whisking, which is a current area of active research [2], [4]–[8], has potential advantages for exploration when other senses such as vision are compromised, for instance, underground, underwater, and in smoky environments [9]. When our robot actively whisks against an object, a "contact" signal is generated due to vibration of the whisker. The contact is sensed by a biomimetic follicle, which records movements of the whisker base. However, actively moving the whisker also generates a sensory signal due to inertial movement of the whisker base in the follicle. Here, we regard this "whisking" signal as self-generated noise because it interferes with the contact signal, which is of primary interest. One simple task that we require the robot to perform is object detection using its whiskers, as a prelude to more complex tasks, such as object recognition and building a spatial map. Currently, the sensitivity of object detection in the robot is poor because the threshold level for detecting contacts must be raised relatively high, to prevent activation by the self-generated whisking signal.

Consideration of the problem of discriminating between self and externally generated sensations is long established in the biological and neurosciences literature (for a discussion, see [10]). As early as the 1950s, von Holst coined the term *reafference principle*[1] to describe self-generated sensations [11]. To solve the reafference problem, von Holst suggested that a copy of the motor command could be retained in the central nervous system, which would be used to cancel the re-afferent signal [11]. This idea has been refined further over the years, leading to the notion that the brain could learn internal dynamical models that predict the sensory consequences of motor actions, thus leading to an ability to discriminate between self-generated and externally generated signals [12]–[16]. An associated interpretation of this principle was made in the study of electric fish, where the notion of reafference was specifically connected to adaptive noise cancelation (ANC) [17]–[19], which is where an adaptive filter learns to cancel additive noise from a signal of interest [20].

Although the uses of predictive models for robotic control are well known (e.g., Smith predictor, generalized predictive control, and self-tuning regulator), it is only more recently that investigation into their related use in recognizing and suppressing self-generated signals has emerged in the field of robotics

[1]In the neurosciences, inputs and outputs to and from the central nervous system are known as afference and efference, respectively. Hence, "reafference" describes sensory signals produced by motor actions of the individual. The term "exafference," on the other hand, describes sensory signals caused by the external environment.

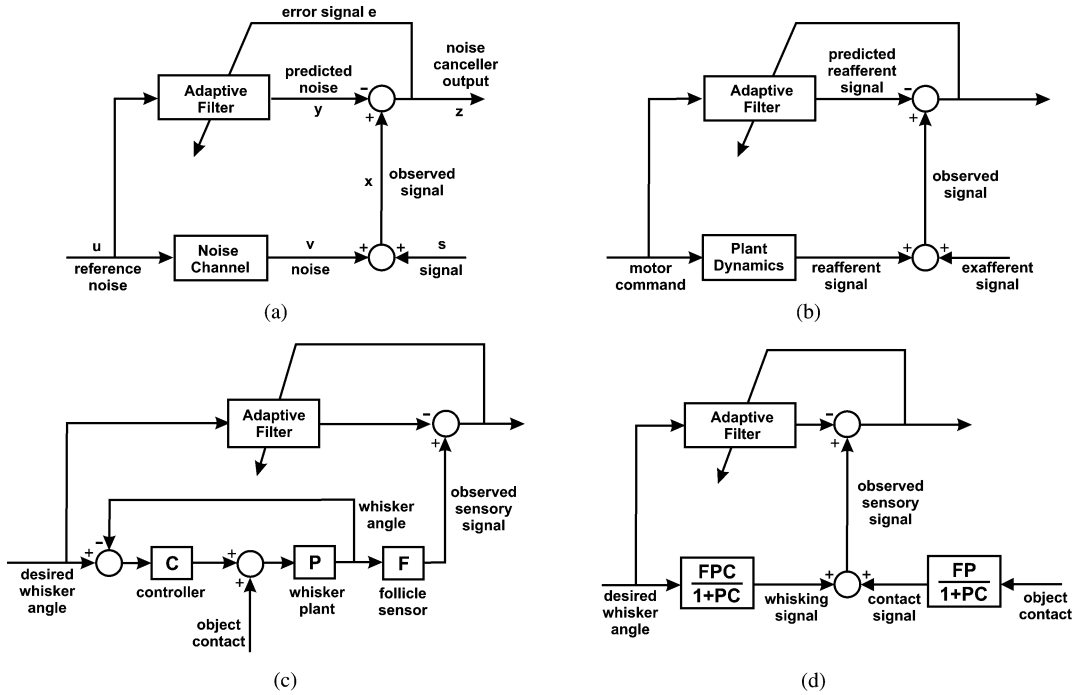

Fig. 1. Link between ANC, the generic cancelation of self-generated sensory signals (using copy of the motor command), and the specific cancelation of the whisking component from combined whisker/contact sensory signals. (a) Classic ANC. The reference noise signal is assumed to be known and correlated with the noise but uncorrelated with the signal. (b) Conceptual mapping of the ANC scheme into the framework of canceling self-generated sensory signals. This scheme uses motor command in analogy to the reference noise. (c) Robot whisker control and sensory scheme with noise canceling adaptive filter. The controller, plant, and follicle sensor are represented by linear transfer functions C, P, and F, respectively. (d) Robot whisking scheme reinterpreted in the architecture of classic ANC.

[21]–[23]. This, we suggest, is likely to be a crucial area of work to improve autonomous robotic behavior. Here, we propose a generic framework to cancel self-generated sensations in robotic systems, motivated from the biological suggestions to utilize motor command to predict the sensory consequences of movement. We show that, for linear systems, our proposed scheme corresponds to classic ANC [20], where the input from the external environment is filtered by a combination of controller and plant dynamics.

For small mobile robotic applications, such as that considered here, it is important to minimize the computational complexity of signal processing algorithms in order to reduce power consumption and maximize energy efficiency. Hence, in this investigation, we use linear filter basis functions to implement the adaptive filter in the noise cancelation scheme. This leads to reduced model order compared with the standard tapped-delay line (TDL) implementation, which is computationally advantageous for embedded applications in autonomous robots. To demonstrate the utility of the scheme, we apply the noise cancelation algorithm to the contact detection problem (described earlier) in our whisking robot. The noise-cancelation algorithm is based on the standard method described in [20]. The key point is that we use a bioinspired method of defining the reference noise as the copy of whisking motor command. This scheme links to the biological perspective on internal models: The robot learns to represent its own movement dynamics. Previously, we have presented elements of this work in abstract form, where the self-generated sensations of the robot rat were canceled using a TDL adaptive filter [24].

The paper is organized as follows. The ANC scheme, adaptive filter structure, and algorithm are derived in Section II. The results from predicting sensory consequences of movement during free-whisking and enhancing contact detection are presented in Section III. A discussion of results is given in Section IV. Finally, the investigation is summarized in Section V.

II. Methods

The noise cancelation problem can be solved optimally using the Wiener filter [25], the principles of which lead to a fixed filter. However, the design of fixed filters relies on *a priori* knowledge of signal statistics and also assumes that the signal will be stationary. The ability to adapt based on changes in task, environment, and robot dynamics (e.g., a broken whisker) is an essential feature of an autonomous robot. Hence, the solution framework we develop here is based on the adaptive filter approach. We first explain the ANC method and then relate it to self-generated noise and, specifically, the whisker contact detection problem. We then present a computationally efficient implementation of the adaptive finite-impulse response (FIR) filter using Laguerre functions (LFs).

A. ANC for Self-Generated Sensory Signals

ANC makes use of a reference noise u to cancel additive noise v from a signal of interest s, where only the combined signal $x = s + v$ is observed [20]; see Fig. 1(a). The key point is that the reference noise is uncorrelated with the signal, but is correlated, via a "noise channel," with the additive signal noise.

An adaptive filter learns the dynamics of the noise channel and produces the output y, which is the noise canceling signal. Therefore, the noise cancelation scheme output z at sample time t is as follows:

$$z_t = x_t - y_t \tag{1}$$

$$z_t = s_t + v_t - y_t. \tag{2}$$

Let us assume that all signals are zero mean and that the reference noise u_t is uncorrelated with s_t but is correlated with v_t; then, by squaring (2) and taking expectations, we obtain an expression for the covariance, or power, in the noise-cancelation scheme output

$$E\left[y_t^2\right] = E\left[s_t^2\right] + E\left[\left(v_t - y_t\right)^2\right]. \tag{3}$$

Inspection of (3) shows that adjustments in the filter output will not affect the signal power $E\left[s_t^2\right]$. Therefore, the power in $E[(v_t - y_t)^2]$ is minimized when the cancelation scheme output power is minimized

$$\min E\left[y_t^2\right] = E\left[s_t^2\right] + \min E\left[\left(v_t - y_t\right)^2\right]. \tag{4}$$

Hence, minimizing the total output power of the cancelation scheme is equivalent to minimizing the output noise power. Therefore, the output of the cancelation scheme may be used as the error signal e_t to drive filter adaptation, i.e., $e_t = z_t$, which minimizes the filter prediction error of the noise in a least-squares sense.

In the context of canceling self-generated noise, we can write down a conceptual model of the self-generated noise cancelation scheme by analogy with Fig. 1(a), replacing the reference noise with motor command, as shown in Fig. 1(b). To obtain the cancelation scheme for the specific case of the whisking robot, it is necessary to consider the robot whisker control scheme and relate that to the generic scheme in Fig. 1(b). The whisker plant is controlled by a PID controller and motor in a negative feedback loop. We model the output of this control loop (whisker angle) as the input to the follicle sensor. We model the contact signal as an additive disturbance to the whisker; it is, therefore, within the feedback loop. Hence, let us assume that each component of the system can be represented by a linear filter, the observed whisker sensory signal can be described as the sum of the two input signals, filtered by follicle, whisker plant, and controller dynamics

$$x_t = G(q)u_t + H(q)d_t \tag{5}$$

where q is the shift operator ($qu_t = u_{t+1}$), d_t is the object contact input signal

$$G(q) = \frac{F(q)C(q)P(q)}{1 + C(q)P(q)} \tag{6}$$

$$H(q) = \frac{F(q)P(q)}{1 + C(q)P(q)} \tag{7}$$

and $F(q), C(q)$, and $P(q)$ are linear discrete-time filters representing the follicle, controller, and plant dynamics, respectively. This scheme is shown in Fig. 1(d), which is clearly related to the original noise-cancelation scheme in Fig. 1(a). In the context of the noise-cancelation scheme, the contact signal corresponds to $s_t = H(q)d_t$, and the whisking signal corresponds to $v_t = G(q)u_t$, which leads to an analogous expression of (2), for the whisker signal cancelation scheme

$$z_t = H(q)d_t + G(q)u_t - y_t. \tag{8}$$

The adaptive filter must, therefore, learn the dynamics of the closed-loop expression $G(q)$ using the whisking motor command input u_t, which we assume is uncorrelated with the contact signals $H(q)d_t$.

B. Adaptive FIR Filter With Least-Mean-Square Learning Rule

Typically, an adaptive FIR filter is used to learn the noise channel dynamics of the reference noise to signal noise transformation, where the filter is described as follows:

$$y_t = \sum_{k=1}^{n} w_t^{(k)} u_{t-k+1} \tag{9}$$

where y_t is the filter output at sample time t (prediction of self-generated noise), u_t is the filter input (copy of motor command), the notation u_{t-k} indicates tap delays of the input signal, $w_t^{(k)}$ is the kth time-varying filter weight, and n is the filter order. The filter can be written compactly in vector notation as follows:

$$y_t = \mathbf{u}_t \mathbf{w}_t \tag{10}$$

where $\mathbf{u}_t = [u_t, \ldots, u_{t-n+1}]$, and $\mathbf{w}_t = [w_1, \ldots, w_n]^T$.

The parameters of the adaptive FIR filter are adapted here by the least-mean-square (LMS) rule of Widrow and Hoff [26] and Widrow and Stearns [27]

$$\mathbf{w}_{t+1} = \mathbf{w}_t + \mu \mathbf{u}_t e_t \tag{11}$$

where μ is a learning rate parameter, e_t is the filter prediction error, and the product term $\mathbf{u}_t e_t$ is a sample estimate of the squared-filter prediction error gradient vector. The learning rate term μ can be a constant, but here, we use normalized LMS (NLMS), where $\mu = \beta / \|\mathbf{u}_t\|^2$ and where β is a constant. The NLMS rule typically increases the rate of convergence [27]. Regarding convergence, subject to the stability of the implementation, the NLMS rule converges to the Wiener filter solution [28].

C. Reducing Model Order of the FIR Filter Using LFs

The FIR filter implemented with a TDL normally requires a large number of parameters, which is undesirable due to excessive computational complexity. The reason for this is that the true system impulse response often decays slowly with respect to the sample rate, requiring many tapped-delays and associated parameters. One method for reducing the order of the FIR filter is to decompose the description of the impulse response into a weighted sum of linear basis functions [29]

$$y_t = \sum_{k=1}^{p} w_t^{(k)} L_k(q, \boldsymbol{\gamma}) u_t \tag{12}$$

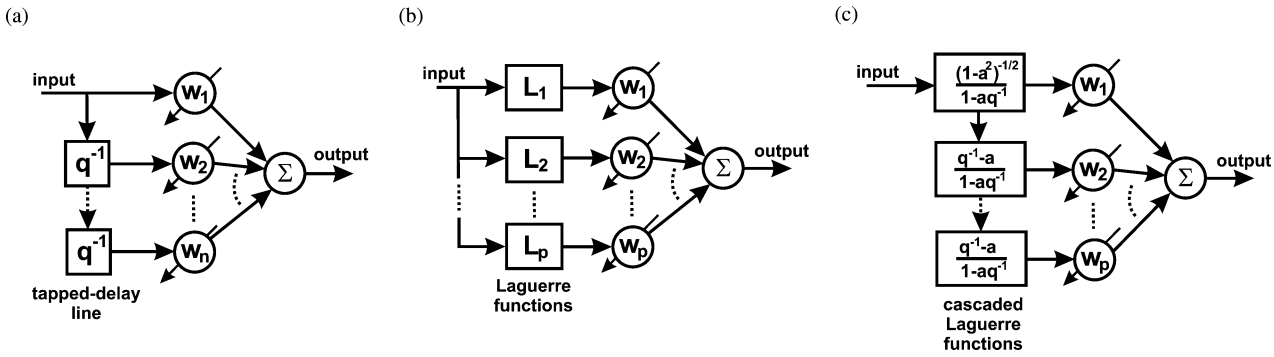

Fig. 2. Various possible structures of the adaptive FIR filter. (a) Standard TDL implementation of the adaptive FIR filter. (b) LF implementation of the adaptive FIR filter. (c) Cascaded LF implementation of the adaptive FIR filter.

where the number of filter weights is p, $L_k(q,\boldsymbol{\gamma})$ is a basis function that is a linear discrete-time filter, and $\boldsymbol{\gamma}$ is the vector of filter parameters. The adaptive filter output can be compactly expressed as follows:

$$y_t = \boldsymbol{\psi}_t \mathbf{w}_t \tag{13}$$

$$\boldsymbol{\psi}_t = \left[L_1(q,\boldsymbol{\gamma})u_t, \ldots, L_p(q,\boldsymbol{\gamma})u_t\right]. \tag{14}$$

The basis functions replace the TDL and, importantly, can greatly reduce the number of model parameters, which are therefore, typically $p \ll n$. The basis functions that we use here have been extensively investigated in the system identification and signal processing literature, namely LFs [30]–[33]. The LFs are attractive for dynamic system descriptions because they form an orthonormal basis for white noise inputs (as do TDLs), yet they are insensitive to the choice of sample rate (unlike TDLs). The sequence of LFs is defined as follows:

$$L_k(q,\boldsymbol{\gamma}) = \frac{\sqrt{(1-a^2)}}{1-aq^{-1}}\left(\frac{q^{-1}-a}{1-aq^{-1}}\right)^{k-1} \quad \text{for } k = 1,\ldots,p \tag{15}$$

where q^{-1} is the backward-shift operator, and the filter parameter vector $\boldsymbol{\gamma}$ is composed of only a single element $\gamma = a$. In principle, other basis functions may be used to describe the FIR filter, such as Kautz functions [31] and generalized bases [34]. However, as will be seen in Section III, LFs describe the data accurately and have the advantage of a simple parameterization (requiring the selection of only one unknown filter parameter a).

The LF parameter a was selected here by use of a separable least-squares algorithm [35]. Separable least squares is commonly applied to optimization problems, where the variables naturally separate into linear and nonlinear sets, improving convergence rate and numerical conditioning [36]. In the case of LFs, the adaptive filter weights $\mathbf{w}$ comprise the linear set of parameters and the filter parameter a is defined as the (only) nonlinear parameter. The optimal filter weights can be estimated (in a batch mode offline, from N samples) by least squares for any given value of a

$$\mathbf{w}_{\mathrm{LS}} = \Psi(a)^{\dagger}\mathbf{x} \tag{16}$$

where $\Psi(a) = \left[\boldsymbol{\psi}_1(a)^T, \ldots, \boldsymbol{\psi}_N(a)^T\right]^T$, $\mathbf{x} = [x_1, \ldots, x_N]^T$, and $\dagger$ indicates the pseudoinverse. As an outline, the weights $\mathbf{w}_{\mathrm{LS}}$ were estimated by least squares within each iteration of a nonlinear optimization of the parameter a, thus avoiding their explicit inclusion in the nonlinear search. The cost function used to optimize the parameter a was the rms filter prediction error. The Nelder–Mead simplex algorithm was applied to solve the nonlinear optimization problem (using the MATLAB function *fminsearch*).

Regarding the online implementation of the LFs in a robotic system, the LFs can be implemented as a cascade of first-order filters. In fact the LFs in (15) are naturally defined as the product of first-order filters; hence, a cascade is simple to implement directly from inspection of (15) in terms of a single parameter a, where the first LF is as follows:

$$\Lambda_1(q,\boldsymbol{\gamma}) = \frac{\sqrt{1-a^2}}{1-aq^{-1}} \tag{17}$$

and the subsequent filters are each defined as follows:

$$\Lambda_2(q,\boldsymbol{\gamma}) = \frac{q^{-1}-a}{1-aq^{-1}}. \tag{18}$$

A cascade of first-order filters has two distinct advantages in comparison with separately implementing each LF (the direct-form). First, the number of multiplications is reduced from $2p(p+1)/2$ in the case of separate LFs to just $2p$ for the cascade form. Second, the cascade form of an infinite-impulse response filter (such as an LF) typically has improved numerical robustness compared with the direct form for finite-word-length implementations [37]. Different possible structures of the adaptive filter are compared in Fig. 2(a)–(c).

D. ANC Algorithm

The ANC algorithm, incorporating the cascade of first-order LF filters and parameter adaptation by NLMS, is described in Algorithm 1. The algorithm requires the specification of three parameters before implementation online, which are 1) the LF filter parameter a; 2) the number of LFs p; and 3) the learning rate parameter β. Selection of these parameters is task specific and is discussed for the whisking robot application in Section III.

The computational complexity of Algorithm 1 is $\mathcal{O}(p)$, where p is the number of LF weights, which is typical of LMS algorithm implementations [27]. This linearity in computational complexity is an attractive feature of LMS adaptation and is

Algorithm 1 Adaptive Self-Generated Noise Cancellation

1: $\psi_t^{(1)} = \Lambda_1(q, \boldsymbol{\gamma})u_t$ {filter input through first LF}
2: **for** $j = 2$ to p **do**
3: $\quad \psi_t^{(j)} = \Lambda_2(q, \boldsymbol{\gamma})\psi_t^{(j-1)}$ {cascade of LFs}
4: **end for**
5: $y_t = \boldsymbol{\psi}_t \mathbf{w}_t$ {adaptive filter output}
6: $z_t = x_t - y_t$ {noise cancellation scheme output}
7: $\mu_t = \frac{\beta}{\boldsymbol{\psi}_t \boldsymbol{\psi}_t^T}$ {learning rate}
8: $\mathbf{w}_{t+1} = \mathbf{w}_t + \mu_t \boldsymbol{\psi}_t z_t$ {parameter adaptation}

TABLE I
COMPUTATIONAL COMPLEXITY (NUMBER OF MULTIPLICATIONS AND DIVISIONS PER ITERATION) FOR ADAPTIVE FILTERING VIA A TDL IMPLEMENTATION COMPARED WITH A CASCADE OF LFS (ALGORITHM 1)

	Tapped-Delay-Line	Cascade of Laguerre Functions
Input Filtering	0	3p
Adaptive Filter Output	n	p
Learning Rate	n+1	p+1
Parameter Adaptation	n	p
Total	3n+1	6p+1

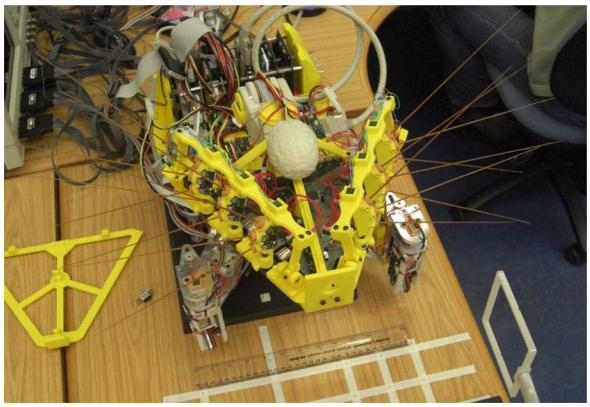

Fig. 3. Whisking robot. SCRATCHbot.

particularly suited to applications in robotic systems, where it is important to minimize computational requirements.

The total computational complexity of Algorithm 1 (using a cascade of LFs) is compared with a TDL equivalent in Table I. We note that although the complexity would be higher for LFs if $p = n$, in fact, for a TDL and LF filter implementation of similar accuracy, typically, $p \ll n$ [31]. Hence, we suggest that use of LFs will often be an attractive option with regard to reducing computational complexity. This point is specifically addressed for the whisking robot application in Section III.

E. Whisking Robot

The whisking robot utilized in this study is a development of the prototype described in [2] and [3]; see Fig. 3. The new whisking robot, i.e., SCRATCHbot [8], has 18 whiskers arranged in three columns of three whiskers per column on each side of the robot head (i.e., nine on each side). Each of the columns are independently actuated using dc motors, providing 120° of rotation (see Fig. 4).

The reference trajectory of each column is currently specified by the operator and controlled using a PID position control algorithm implemented in a local microcontroller (with a sample rate of 200 Hz). Each of the plastic whiskers [made from acrylonitrile butadiene styrene (ABS)] has a small magnet bonded to the base that, in turn, is mounted into a flexible polymer follicle. Any movement of the magnet is monitored in two dimensions using a Hall effect sensor located inside the follicle. Therefore, any deflections of the whisker shaft are represented as displacement vectors at the base.

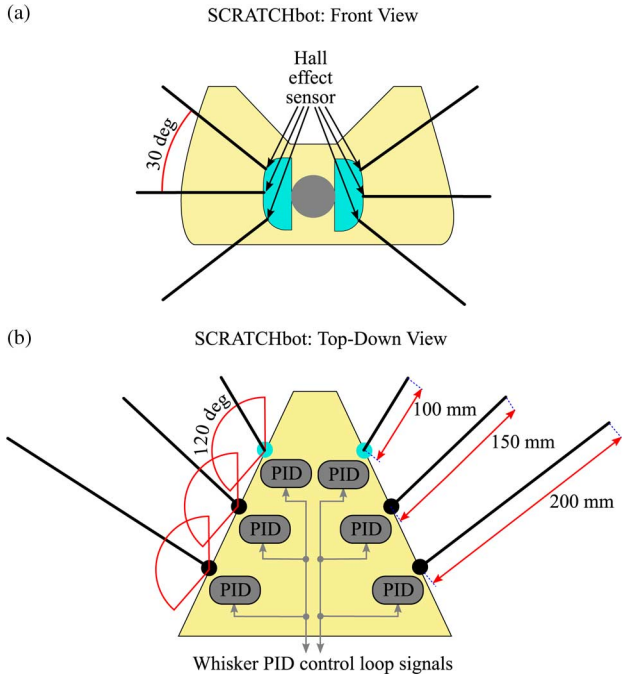

Fig. 4. Diagram of SCRATCHbot head. (a) (Front view) Front two columns of whiskers are illustrated. The three rows of whiskers on each side of the head are spread by 30°. The movement of each whisker activates a Hall effect sensor that gives a measure of whisker displacement. (b) (Top-down view) All six columns of whiskers are illustrated. Each column of whiskers is independently actuated by a dc motor under PID control. Each column can move through 120° of rotation. The lengths of the whiskers decrease from front to back of the head (100–200 mm).

By taking inspiration from mammalian vibrissal fields, the lengths and thicknesses of the whiskers vary across the array, with the longer thicker whiskers located toward the rear. The results of this study were taken from a 200-mm-long whisker shaft with a circular cross section of 2 mm diameter at the base, tapering linearly to 0.6 mm diameter at the tip.

F. Experiment Design

A single whisker on the robot (rear column, middle row of the 3×3 array) was driven in two separate experiments, without contacts (free-whisking) and with contacts, where each run was of 2 min in duration. Each dataset was collected under head fixed conditions. The free-whisking data was used to design the LFs prior to the contact detection task. In the contact detection experiment, the contact object (a flexible plastic rod that is 80 mm long and 1.5 mm in diameter) was held in the path of the whisker at random times and removed after contact. Contact times of the whisker were obtained with coarse accuracy (to the nearest second) by use of a video recording of the

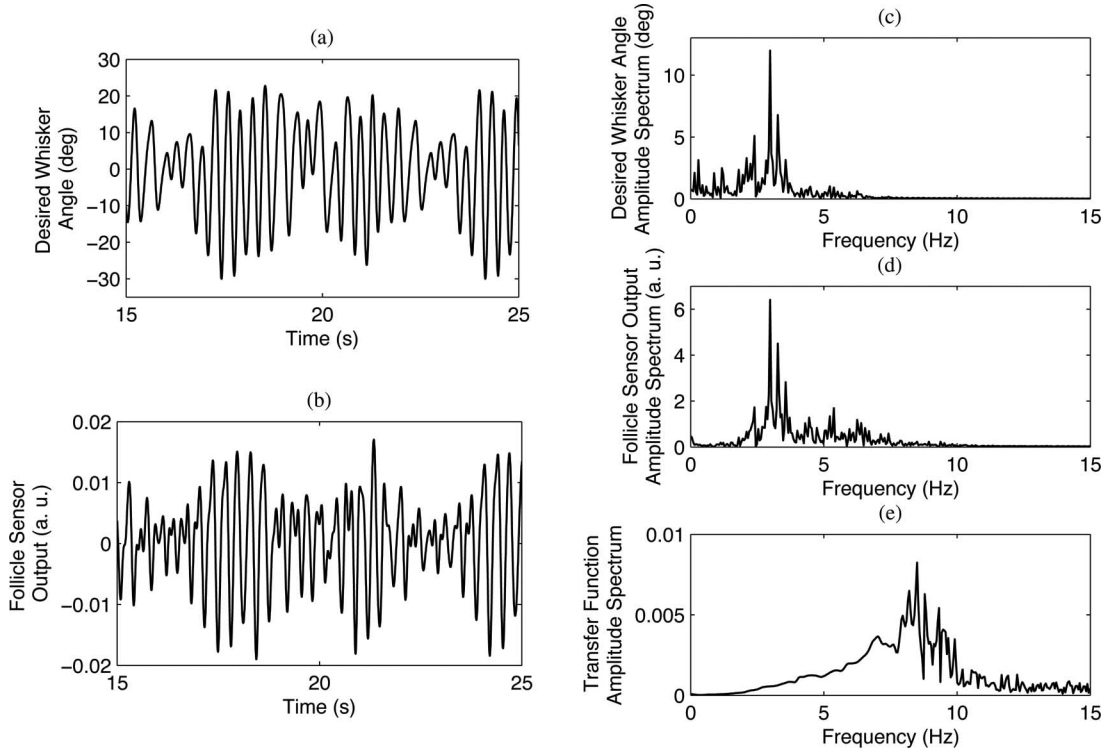

Fig. 5. Robotic whisker input–output signals (desired whisker angle and follicle sensor output, respectively). (a) Desired whisker angle signal, zoomed on the time-axis to a typical 10-s segment. The desired whisker angle signal was obtained from real-rat whisking recorded by Towal and Hartmann [38]. (b) Follicle sensor output signal, zoomed on the time-axis to a typical 10-s segment. (c) Desired whisker angle amplitude spectrum. (d) Follicle sensor output amplitude spectrum. (e) Robotic whisker transfer function amplitude spectrum obtained from the ETFE.

experiment. Precise contact times of the whisker were obtained from applying the noise cancelation algorithm to the data and visually inspecting the resulting "clean" signal, with reference to the contact times obtained from the video recording. Each input–output dataset was processed and analyzed offline using MATLAB.

We drove the whiskers of the robot with an input signal (desired whisker angle) obtained from real-rat whisking recorded by Towal and Hartmann [38]. Two typical free-whisking trials of $\sim$1.5 s in duration were concatenated together to form an input signal of $\sim$3 s. The original signals had a strong periodic component in the whisking at $\sim$8 Hz. We scaled the whisking signal to reflect the larger size of the robot rat (compared with an actual rat). Therefore, we lowered the whisking rate by redefining the sample rate from 250 to 100 Hz, thereby shifting the whisking rate down by a factor of 2.5 so that the strong periodic component of whisking occurred at $\sim$3 Hz. The resulting signal, of duration $\sim$7.5 s, was looped for 2 min to form the input signal used in the free-whisking and contact experiments.

The characteristics of the input–output data from the robot whisker plant (desired whisker angle and follicle sensor output, respectively) are shown in Fig. 5(a)–(d) from free-whisking. The dynamic characteristics of the robot whisker plant, which are equivalent to the transfer function $G(q)$ defined in (6), are described in Fig. 5(e) by the empirical transfer function estimate (ETFE) [29]. The ETFE is the ratio between the Fourier transforms of the output and input and was obtained in this case by the MATLAB function *tfestimate*, which uses Welch's method to obtain the estimate [29]. The input–output signals were sampled from the robot at 200 Hz and low-pass filtered at 5 Hz to attenuate nonlinear harmonics in the output signal. In principle, it would be possible to describe these nonlinearities with a nonlinear FIR filter that was outside the scope of this investigation and did not affect the main result of enhancing contact detection.

III. Results

This section presents results for the adaptive filter design and application to the task of enhancing whisker contacts in the presence of self-generated noise. The task was to dynamically model the whisker plant (desired whisker angle to follicle sensor output transformation) and use this model to cancel the self-generated sensory signal using an adaptive FIR filter (see Algorithm 1). The results are divided into three sections: LF selection, prediction of sensory consequences of movement, and contact detection.

A. LF Structure Detection

The LF structure detection task was composed of selecting two parameters: the filter parameter a and the number of LFs p. The number of LFs p was selected first by comparing the FIR filter prediction of the follicle sensor output signal for different numbers of LFs. The optimal fit of each LF filter was obtained in a batch mode using least squares. We fitted 1 to 6 LFs (using the free-whisking data) with the filter parameter a systematically varied from 0.5 to 0.96. The rms fit error was compared across

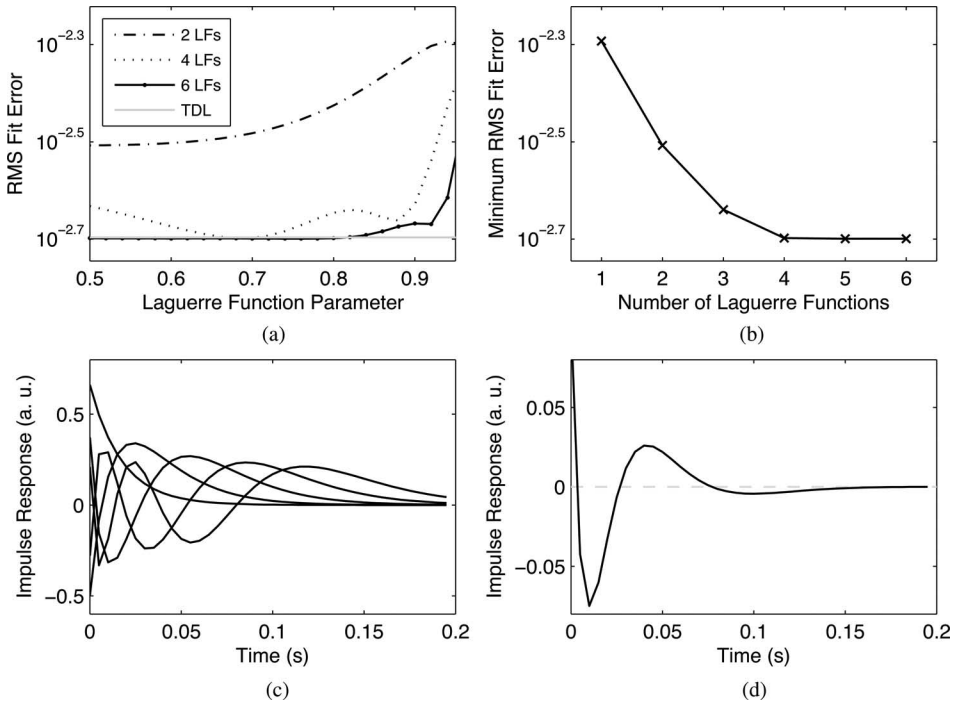

Fig. 6. Structure detection for the LFs. (a) Comparison of FIR filters composed of two to six LFs in terms of rms fit error along with the fit error of a TDL FIR filter (40 taps), where the LF parameter a was varied systematically between 0.5 and 0.96. (b) Comparison of LF FIR filters in terms of minimum rms fit error. (c) Impulse responses of the Laguerre basis functions 1 to 5, which are weighted and summed to form the whisker plant impulse response (where $a = 0.75$). (d) Whisker plant impulse response described by the LF filter (5 LFs) obtained from the separable least-squares fit to the free-whisking data (where $a = 0.75$).

the different numbers of basis functions and selected results are shown in Fig. 6(a). We found that at least four LFs were required to model the dynamics of the whisker plant, based on inspection of the knee-point in Fig. 6(b). Although the accuracy of 4 LFs was similar to five LFs, we found that the fit error was more sensitive to the choice of a when using four LFs. Hence, we selected $p = 5$.

After selecting the number of LFs, the parameter a was estimated using a separable least-squares algorithm as described in Section II (where the choice of the single parameter a defined the dynamics of all LFs). The optimal parameter estimate was $a = 0.75$. The impulse responses of the five selected LFs with optimal parameter estimate $a = 0.75$ are shown in Fig. 6(c). The impulse response of the whisker plant (identified by the separable least-squares algorithm) is plotted in Fig. 6(d), which shows that the response is mildly oscillatory and decays after 200 ms.

Only five LFs were required here to model the whisker plant dynamics. A comparable filter length implemented by a TDL would require 40 taps. Hence, the LF implementation resulted in a significant reduction in model order with a corresponding reduction in computational complexity. For this case, the computational complexity of the LF implementation was just 31 multiplications and divisions compared with 121 for the TDL (calculated from the totals in Table I). This reduction in number of operations of 74% scales with the number of whiskers (due to the fact that each whisker requires a separate instance of the cancelation algorithm). To illustrate the benefit of using the LFs, recalling that SCRATCHbot has 18 whiskers in total, in the time it would take to process just four whiskers using a TDL, it would be possible to process all 18 whiskers using the LF implementation of Algorithm 1.

B. Prediction of Sensory Consequences of Movement

The adaptive filter was required to learn the whisker plant dynamics online (as opposed to the offline identification used to select the LFs, discussed earlier). For the case of free-whisking (i.e., no contacts), the adaptive filter output y_t should closely match the output of the follicle sensor x_t. Therefore, after defining the LFs, we ran the ANC algorithm (see Algorithm 1) on the free-whisking data to confirm that the adaptive filter could accurately learn the whisker plant dynamics. The user-defined parameters in Algorithm 1 were set to $a = 0.75$, $p = 5$, and $\beta = 0.01$. The adaptive filter weights were initialized to zero.

We found that after filter convergence on the free-whisking data the prediction accuracy of the self-generated noise was high. Fig. 7(a) and (b) compares the filter output y_t with the follicle output x_t, at the beginning and end of learning, respectively. The variance accounted for[2] (VAF) obtained from the final 20 s of free-whisking data was VAF = 0.94.

C. Contact Detection

Apart from the choice of LF function parameter a and the number of LFs p, the only other user-defined parameter

[2]The VAF metric is a measure of model-fit quality, where VAF = 1–var(e)/var(y), where e is the fit error, and y is the target data. Hence, a VAF ≈ 1 implies that the model fit is good because the normalized error variance is close to zero. The VAF is also known as the coefficient of determination or r-squared value.

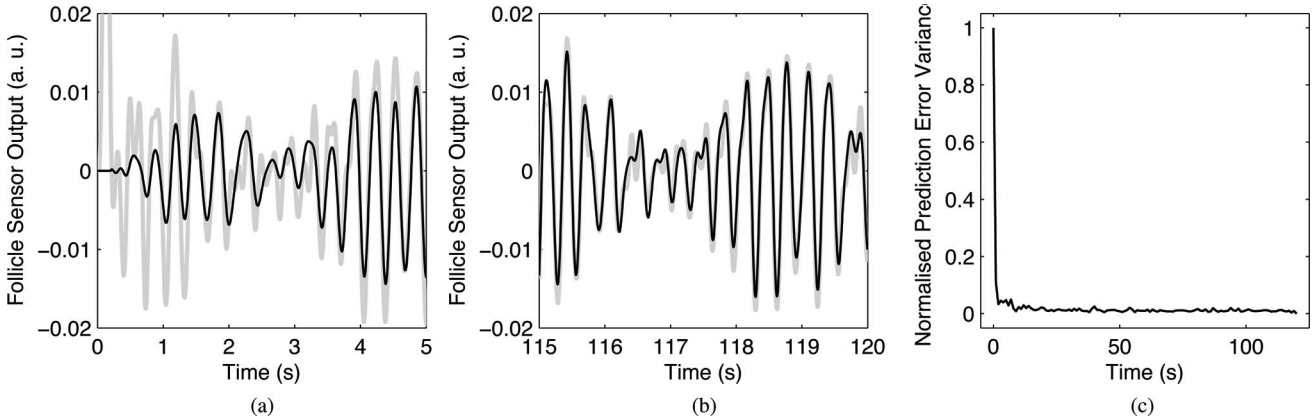

Fig. 7. Prediction of the sensory consequences of active whisking, where the adaptive filter learns over time to predict the whisker follicle sensor output. (a) Start of learning (first 5 s), where adaptive filter prediction is in black and follicle sensory signal is in grey. (b) End of learning (final 5 s), where adaptive filter prediction is in black, and follicle sensory signal is in grey. (c) Normalized variance of the adaptive filter prediction error (where each sample of the variance is taken over 1 s).

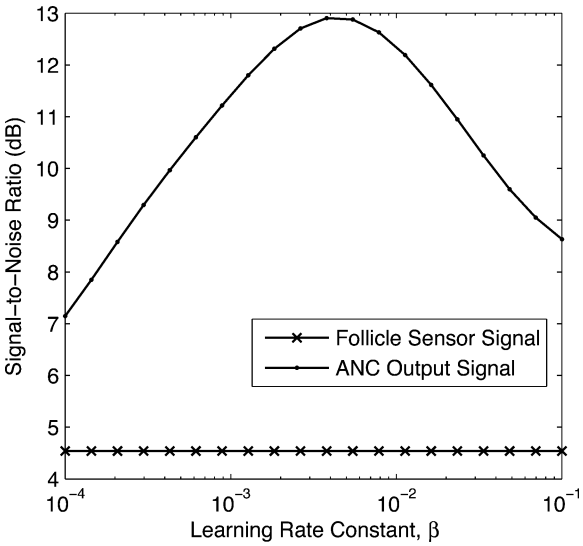

Fig. 8. Variation in SNR for different rates of learning in the ANC scheme with baseline comparison with the SNR obtained from the follicle sensor output. Results were obtained from one presentation of the contact data to the noise cancelation algorithm.

necessary to implement Algorithm 1 was the learning rate constant β. We investigated choice of learning rate parameter with respect to performance in the contact detection task. The metric used to measure performance was SNR. The signal power in the SNR measure P_s was defined as the variance of the signal segment 200 ms before and after a contact. The noise power in the SNR measure P_n was defined as the variance of the remainder of the signal after removing the contact segments. Hence, SNR was defined as $\text{SNR} = 10\log_{10}(P_s/P_n)$. The SNR measure was obtained after applying Algorithm 1 to the contact data, varying the learning rate between 10^{-4} and 10^{-1}. The optimal learning rate parameter that maximized SNR was found to be $\beta \approx 0.004$ (see Fig. 8). The limiting factor on faster learning (i.e., for $\beta > 0.004$) appeared to be due to contacts disrupting adaptation. However, stability was guaranteed, even in the presence of these contacts because the filter input was stationary and uncorrelated with object contacts [27].

After selecting the learning parameter β, we ran Algorithm 1 on the contact data (described in Section II-F) to assess the utility of the noise-cancelation scheme. The contact detection experiment was of duration 2 min, corresponding to $N = 24\,000$ samples at the sample rate of 200 Hz. Parameter adaptation took place at each sample time. Separate analysis on contact-free data showed that at this learning rate prediction accuracy was over 90% within 2 s of adaptation. Contacts in the whisking signal were well amplified (compared with the raw sensory signal) as errors in prediction, as shown in Fig. 9(a) and (b). It is apparent from a visual inspection of Fig. 9(a) that many of the contacts are effectively hidden within the self-generated noise. By comparison, a visual inspection of Fig. 9(b) emphasizes the utility of the noise cancelation scheme by revealing the location of contacts in the ANC output.

The purpose of the noise cancelation scheme was to enhance contact detection in comparison to using the raw follicle output signal. The method we used for detecting contacts was to apply a threshold to both the follicle output and noise cancelation scheme output. Signal values that exceeded the threshold were classified as contacts. In order to assess the improvement in detecting contacts by the noise cancelation scheme, we used a measure known as the receiver operating characteristic (ROC) curve, which is widely used in classification problems [39]. The ROC curve plots the false positive rate against the true positive rate (where the false and true positive rates are the normalized number of true positives and false positives, respectively). We defined the maximum possible number of false positives as the number of forward whisks (due to the fact that each whisk could have potentially signalled a contact). We obtained the ROC curve by systematically varying the contact detection threshold from 0 to 1.1, applying each threshold to the absolute values of the normalized follicle output and cancelation scheme output (i.e., the signals shown in Fig. 9) and counting the number of resulting true and false positives corresponding to each signal. The ROC curve showed that for the raw signal (follicle sensor output), a true positive rate of 0.95 could only be obtained at the expense of a false positive rate of $\sim$0.53 (see Fig. 10), which is poor performance. By contrast, the clean signal (noise

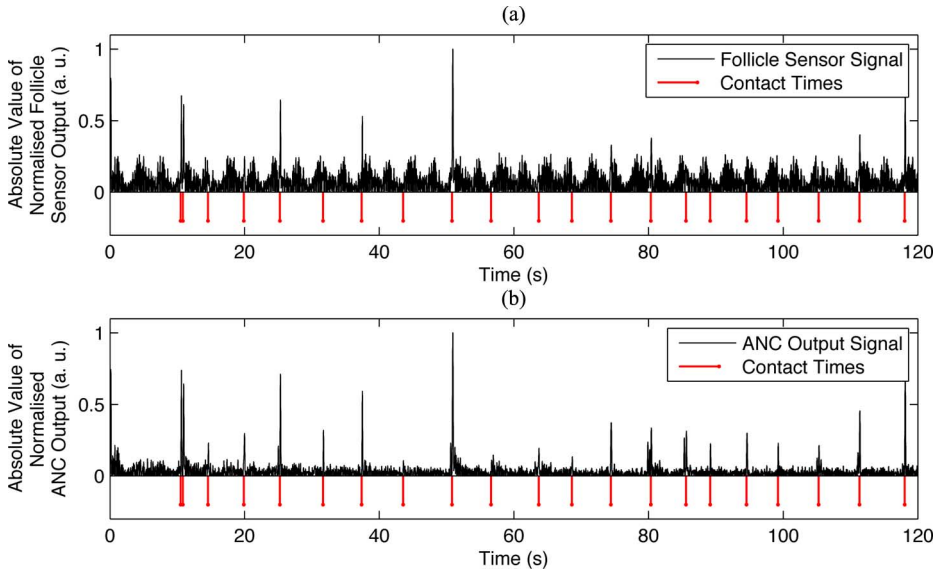

Fig. 9. ANC scheme applied to the problem of contact detection from the robot whisker sensory signal. (a) Absolute value of the whisker follicle sensor output, normalized by the peak signal value. (b) Absolute value of the ANC scheme output, normalized by the peak signal value.

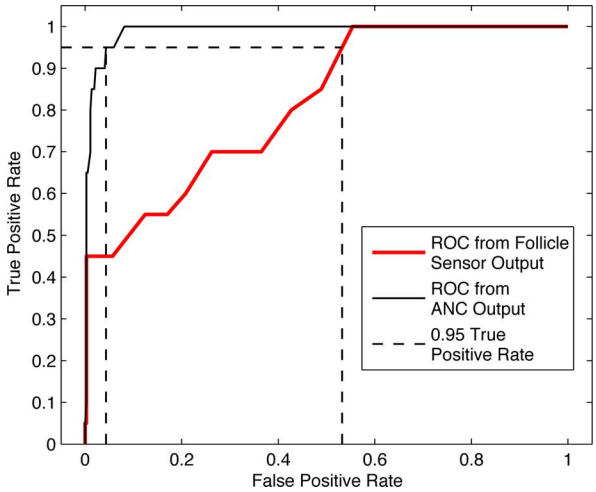

Fig. 10. ROC curve that describes false positive versus true positive rates of contacts detected at varying threshold levels from 1) the raw follicle sensor output signal and 2) the clean signal generated by the ANC scheme.

cancelation scheme output) gave a true positive rate of 0.95 for a false positive rate of only ∼0.04 (see Fig. 10). Hence, the use of the cancelation scheme greatly enhanced contact detection for this dataset.

IV. Discussion

A. Improved Contact Detection by ANC

We found that the noise cancelation scheme based on the biological principle of using copy of the motor command worked as expected from the theory. The adaptive filter successfully learnt a model of the robot whisker controller-plant dynamics (demonstrated by the adaptive filter learning to predict the sensory consequences of movement during free-whisking). We showed that the particular adaptive FIR filter implementation we chose (cascaded LFs) reduced computational complexity in comparison with a TDL. We tested the algorithm on contact detection during active robot whisking, where we showed that the use of the noise-cancelation scheme led to a much improved ratio of true positives to false positives in comparison with using the raw sensory signal.

Hence, the algorithm (see Algorithm 1) that we have developed here is well suited to applications in autonomous robotics because 1) it should lead to improved discrimination between self-generated and externally generated signals in general robotic tasks (i.e., not limited to whisking); 2) the implementation is adaptive and, hence, suitable for online learning; and 3) the algorithm is relatively computationally inexpensive (linear in the model order, where order will typically be small due to the use of LFs). As in the case of generic LMS adaptation schemes, the instance of the noise-cancelation algorithm presented here is stable and convergent, provided the learning rate is within acceptable bounds and able to track slowly time-varying systems [28].

B. Computationally Efficient Algorithm for Mobile Robotic Platforms

The SCRATCHbot platform, like all autonomous mobile robotic platforms, has a limited onboard power supply. A considerable amount of this power is required by the actuators and processors distributed across the platform to control each degree of freedom as well as the single board computer (SBC) and field-programmable gate array (FPGAs) used for signal processing, higher level planning, and control. Consequently, the chosen SBC represents a compromise between power consumption and computational performance. To overcome the computational constraints of the platform, external processors could be employed and integrated using wireless communication. However, the data bandwidths and latencies of conventional wireless protocols do not currently satisfy the requirement for the

proposed noise-cancelation scheme. Computational efficiency of onboard signal processing algorithms is, therefore, of utmost importance. Here, we have developed a noise cancelation algorithm that focused on reduction of computational complexity by the use of LFs, rather than the commonly used TDL. The number of computations in this case was reduced by 74% (from 121 to 31 for one whisker output), which is a highly beneficial improvement for onboard processing.

C. Possible Neural Substrates of a Contact Detection Scheme in the Rat

Given the success of the cancelation scheme considered here, based on adaptive filtering, it is natural to ask whether there exists a comparable functional system in whisking animals, such as rat. It has been reported that rat free-whisking (i.e., with no contacts) generates a sensory signal [40], [41]. This signal is analogous to the self-generated signal observed in our whisking robot. Therefore, it is possible that a similar problem of discrimination between self- and externally generated signals exists in the rat.

In a parallel theme of work, we are currently investigating the possibility that the cerebellum is involved in a biological cancelation scheme, where the cerebellum is the structure that performs the role of the adaptive filter [24], [42]. The cerebellum is a natural candidate for this role because of the resemblance of the cerebellar microcircuit to the adaptive filter [43], [44]. The cerebellum has also been particularly associated with the concept of learning internal dynamical models [12], [13], [45].

The adaptive filter is a widely used model of cerebellar processing and the nature of the basis functions used in biological systems is an area of active research. Marr and Albus originally proposed that the granule cell layer implemented a basis that performed a massive expansion recoding of cerebellar (mossy fiber) inputs [46], [47]. An important question is whether the Marr–Albus hypothesis of granule cell layer function is consistent with recent electrophysiological evidence thought to suggest a modest role for granular layer transformation (references in [48]). If this proves to be the case, then bases, such as the LFs used here, which are much more efficient (as well as more biologically plausible) than TDLs, may have applications to biological systems.

V. Summary

This investigation has addressed the problem of canceling self-generated robotic sensory signals in a generic framework. The choice of reference noise as input to the adaptive filter in the cancelation scheme was motivated by the biological observation that one may use a copy of motor commands as input to an internal model in order to predict sensory consequences of movement. The algorithm was based on adaptive FIR filtering, where the filter input was first transformed by LFs (rather than TDLs) to reduce the filter order and, in turn, the computational complexity. The cancelation scheme was applied to self-generated sensory signals in a whisking robot. We showed that the cancelation scheme greatly enhanced contact detection on signals recorded from robot whisker contacts, dramatically reducing the false positive rate.

Acknowledgment

The authors would like to thank B. Towal and M. Hartmann for the rat whisking data that was used to generate the input signal to drive the robot whisker.

References

[1] R. Bajcsy, "Active perception," *Proc. IEEE*, vol. 76, no. 8, pp. 996–1005, Aug. 1988.
[2] M. J. Pearson, A. G. Pipe, C. Melhuish, B. Mitchinson, and T. J. Prescott, "Whiskerbot: A robotic active touch system modeled on the rat whisker sensory system," *Adapt. Behav.*, vol. 15, no. 3, pp. 223–240, 2007.
[3] C. W. Fox, B. Mitchinson, M. J. Pearson, A. G. Pipe, and T. J. Prescott, "Contact type dependency of texture classification in a whiskered mobile robot," *Auton. Robots*, vol. 26, no. 4, pp. 223–239, 2009.
[4] M. J. Hartmann, "Active sensing capabilities of the rat whisker system," *Auton. Robots*, vol. 11, no. 3, pp. 249–254, 2001.
[5] D. Kim and R. Moller, "Biomimetic whiskers for shape recognition," *Robot. Auton. Syst.*, vol. 55, no. 3, pp. 229–243, 2007.
[6] G. R. Scholz and C. D. Rahn, "Profile sensing with an actuated whisker," *IEEE Trans. Robot. Autom.*, vol. 20, no. 1, pp. 124–127, Feb. 2004.
[7] J. H. Solomon and M. J. Z. Hartmann, "Artificial whiskers suitable for array implementation: Accounting for lateral slip and surface friction," *IEEE Trans. Robot.*, vol. 24, no. 5, pp. 1157–1167, Oct. 2008.
[8] T. J. Prescott, M. J. Pearson, B. Mitchinson, J. C. W. Sullivan, and A. G. Pipe, "Whisking with robots," *IEEE Robot. Autom. Mag.*, vol. 16, no. 3, pp. 42–50, Sep. 2009.
[9] M. J. Hartmann and J. H. Solomon, "Robotic whiskers used to sense features," *Nature*, vol. 443, pp. 525–525, 2006.
[10] K. E. Cullen, "Sensory signals during active versus passive movement," *Curr. Opin. Neurobiol.*, vol. 14, no. 6, pp. 698–706, 2004.
[11] E. von Holst, "Relations between the central nervous system and the peripheral organs," *Br. J. Animal Behav.*, vol. 2, no. 3, pp. 89–94, 1954.
[12] S. J. Blakemore, S. J. Goodbody, and D. M. Wolpert, "Predicting the consequences of our own actions: The role of sensorimotor context estimation," *J. Neurosci.*, vol. 18, no. 18, pp. 7511–7518, 1998.
[13] S.-J. Blakemore, D. Wolpert, and C. Frith, "Central cancellation of self-produced tickle sensation," *Nat. Neurosci.*, vol. 1, no. 7, pp. 635–640, 1998.
[14] M. I. Jordan and D. E. Rumelhart, "Forward models: Supervised learning with a distal teacher," *Cognitive Sci.*, vol. 16, pp. 307–354, 1992.
[15] R. C. Miall and D. M. Wolpert, "Forward models for physiological motor control," *Neural Netw.*, vol. 9, pp. 1265–1279, 1996.
[16] D. M. Wolpert, Z. Ghahramani, and M. I. Jordan, "An internal model for sensorimotor integration," *Science*, vol. 269, no. 5232, pp. 1880–1882, 1995.
[17] C. C. Bell, J. C. Montgomery, D. Bodznick, and J. Bastian, "The generation and subtraction of sensory expectations within cerebellum-like structures," *Brain Behav. Evol.*, vol. 50, pp. 17–31, 1997.
[18] J. C. Montgomery and D. Bodznick, "An adaptive filter that cancels self-induced noise in the electrosensory and lateral line mechanosensory systems of fish," *Neurosci. Lett.*, vol. 174, pp. 145–148, 1994.
[19] N. B. Sawtell and A. Williams, "Transformations of electrosensory encoding associated with an adaptive filter," *J. Neurosci.*, vol. 28, pp. 1598–1612, 2008.
[20] B. Widrow, J. R. Glover, J. M. McCool, J. Kaunitz, C. S. Williams, R. H. Hearn, J. R. Zeidler, E. Dong, and R. C. Goodlin, "Adaptive noise cancelling: Principles and applications," *Proc. IEEE*, vol. 63, no. 12, pp. 1692–1716, Dec. 1975.
[21] K. Gold and B. Scassellati, "Using probabilistic reasoning over time to self-recognize," *Robot. Auton. Syst.*, vol. 57, no. 4, pp. 384–392, 2009.
[22] P. Manoonpong and F. Worgotter, "Efference copies in neural control of dynamic biped walking," *Robot. Auton. Syst.*, pp. 1140–1153, 2009.
[23] T. Mizumoto, R. Takeda, K. Yoshii, K. Komatani, T. Ogata, and H. G. Okuno, "A robot listens to music and counts its beats aloud by separating music from counting voice," in *Proc. IEEE/RSJ Int. Conf. Intell. Robots Syst.*, Nice, France, 2008, pp. 1538–1543.
[24] S. R. Anderson, J. Porrill, M. J. Pearson, A. G. Pipe, T. J. Prescott, and P. Dean, "Cerebellar-inspired forward model of whisking enhances contact detection by vibrissae of robot rat," in *Soc. Neurosci. Abst.*, no. 77.2, Chicago, IL, 2009.
[25] N. Wiener *Extrapolation, Interpolation, and Smoothing of Stationary Time Series*, New York: Wiley, 1949.

[26] B. Widrow and M. Hoff, "Adaptive switching circuits," in *IRE WESCON Conv. Rec.*, vol. 4, New York, 1960, pp. 96–104.
[27] B. Widrow and S. D. Stearns, *Adaptive Signal Processing*. Englewood Cliffs, NJ: Prentice-Hall, 1985, 2010.
[28] D. T. M. Slock, "On the convergence behaviour of the LMS and normalised LMS algorithms," *IEEE Trans. Signal Process.*, vol. 41, no. 9, pp. 2811–2825, Sep. 1993.
[29] L. Ljung, *System Identification - Theory for the User*, 2nd ed. Upper Saddle River, NJ: Prentice Hall, 1999.
[30] R. E. King and P. N. Paraskevopoulos, "Parametric identification of discrete-time SISO systems," *Int. J. Control*, vol. 30, no. 6, pp. 1023–1029, 1979.
[31] B. Wahlberg, "System identification using Laguerre models," *IEEE Trans. Autom. Control*, vol. 36, no. 5, pp. 551–562, May 1991.
[32] G. W. Davidson and D. D. Falconer, "Reduced complexity echo cancellation using orthonormal functions," *IEEE Trans. Circuits Syst.*, vol. 38, no. 1, pp. 20–28, Jan. 1991.
[33] G. Mandyam and N. Ahmed, "The discrete Laguerre transform: Derivation and applications," *IEEE Trans. Signal Process.*, vol. 44, no. 12, pp. 2925–2930, Dec. 1996.
[34] P. S. C. Heuberger, P. M. J. Van den Hof, and O. H. Bosgra, "A generalized orthonormal basis for linear dynamical systems," *IEEE Trans. Autom. Control*, vol. 40, no. 3, pp. 451–465, Mar. 1995.
[35] L. S. H. Ngia, "Separable nonlinear least-squares methods for efficient off-line and on-line modeling of systems using Kautz and Laguerre filters," *IEEE Trans. Circuits Syst. II*, vol. 48, no. 6, pp. 562–579, Jun. 2001.
[36] G. H. Golub and V. Pereyra, "The differentiation of pseudo-inverses and non-linear least squares problems whose variables separate," *SIAM J. Numerical Anal.*, vol. 10, no. 2, pp. 413–432, 1973.
[37] J. G. Proakis and D. G. Manolakis, *Digital Signal Processing*, 3rd ed. Englewood Cliffs, NJ: Prentice-Hall, 1996.
[38] R. B. Towal and M. J. Hartmann, "Right-left asymmetries in the whisking behavior of rats anticipate head movements," *J. Neurosci.*, vol. 26, no. 34, pp. 8838–8846, 2006.
[39] T. Fawcett, "An introduction to ROC analysis," *Pattern Recognit. Lett.*, vol. 27, pp. 861–874, 2006.
[40] M. Szwed, K. Bagdasarian, and E. Ahissar, "Encoding of vibrissal active touch," *Neuron*, vol. 40, no. 3, pp. 621–630, 2003.
[41] S. C. Leiser and K. A. Moxon, "Responses of trigeminal ganglion neurons during natural whisking behaviours in the awake rat," *Neuron*, vol. 53, pp. 117–133, 2007.
[42] S. R. Anderson, M. J. Pearson, J. Porrill, T. Pipe, T. Prescott, and P. Dean, "Does the cerebellum cancel self-induced noise in whisker sensory signals?," in *Barrels XXI Abst.*, Baltimore, MD, 2008, pp. 26–27.
[43] M. Fujita, "Adaptive filter model of the cerebellum," *Biological Cybern.*, vol. 45, pp. 195–206, 1982.
[44] P. Dean and J. Porrill, "Adaptive filter models of the cerebellum: Computational analysis," *Cerebellum*, vol. 7, pp. 567–571, 2008.
[45] R. C. Miall, L. O. D. Christensen, O. Cain, and J. Stanley, "Disruption of state estimation in the human lateral cerebellum," *PLOS Biol.*, vol. 5, no. 11, pp. 2733–2744, 2007.
[46] D. Marr, "A theory of cerebellar cortex," *J. Physio. (London)*, vol. 202, pp. 437–470, 1969.
[47] J. S. Albus, "A theory of cerebellar function," *Math. Biosci.*, vol. 10, pp. 25–61, 1971.
[48] P. Dean, J. Porrill, C.-F. Ekerot, and H. Jorntell, "The cerebellar microcircuit as an adaptive filter: Experimental and computational evidence," *Nature Rev. Neurosci.*, vol. 11, pp. 30–43, 2010.

Sean R. Anderson received the M.E. degree in control systems engineering from the Department of Automatic Control and Systems Engineering, University of Sheffield, Sheffield, U.K., in 2001 and the Ph.D. degree from the Department of Chemical and Process Engineering, University of Sheffield, in 2005.

From 2005 to 2010, he was a Postdoctoral Research Associate with the Centre for Signal Processing in Neuroimaging and Systems Neuroscience, University of Sheffield, where he was involved in investigating eye movement control and subsequently active touch [as part of the Active Touch Laboratory (ATL@S)]. He is currently with the Department of Automatic Control and Systems Engineering, University of Sheffield, where he is engaged in systems biology. His research interests include nonlinear system identification (with applications in biology), optimal and adaptive control in biological systems, and the application of bioinspired control to robotic systems.

Martin J. Pearson received the Ph.D. degree from the University of the West of England, Bristol, U.K., in 2008.

He is currently a Full-time Postdoctoral Research Fellow with the Bristol Robotics Laboratory, where he is engaged with neuroscientists and ethologists from around the world to understand the rodent whisker active touch sensory system. His research interests include the design and development of robotic hardware to evaluate bioinspired models and the design of real-time, embedded reconfigurable hardware-based processing architectures to implement detailed spiking neural network models.

Anthony Pipe received the Ph.D. degree from the University of the West of England, Bristol, U.K., in 1997.

He is currently the Deputy Director of the Bristol Robotics Laboratory and a Professor with Robotics and Autonomous Systems, Bristol. His research interests include advanced topics for all types of robots but, particularly, physical/behavioral safety aspects of humanoid service robotics and biologically plausible models of mammalian brain function, particularly those embedded in the real-time feedback robot control.

Tony Prescott received the M.A. degree in psychology from University of Edinburgh, Edinburgh, U.K., the M.Sc. degree in artificial intelligence from University of Aberdeen, Aberdeen, U.K., and the Ph.D. degree from the Department of Psychology, University of Sheffield, Sheffield, U.K., in 1994. His research was focused on learning.

He is a currently a Professor of cognitive neuroscience with the Department of Psychology, University of Sheffield. He is also a Permanent Research Fellow with the Bristol Robotics Laboratory, Bristol, U.K. He has authored more than 60 publications in psychology, neuroscience, computational modeling, and robotics. His research interests include the biological and brain sciences and is particularly concerned with understanding the evolution, development, and function of natural intelligence and the investigation of computational neuroscience models of animal and human intelligence and in testing these models in biomimetic robots.

Paul Dean received the M.A. degree in physiology with psychology from the University of Cambridge, Cambridge, U.K., and the D.Phil. degree from the University of Oxford, Oxford, U.K.

He is currently a Professor with the Department of Psychology and a Member of the Centre for Signal Processing in Neuroimaging and Systems Neuroscience, University of Sheffield, Sheffield, U.K. . His research interests include producing computational models of neural systems that are based on both biological data and developments in control engineering, signal processing, and robotics, which serve as a vehicle for two-way communication between biological and physical sciences, allowing roboticists to use new discoveries in biology and biologists to interpret their findings in light of current developments in signal processing.

John Porrill received the Ph.D. degree from the University of Cambridge, Cambridge, U.K. His research focused on topics in classical general relativity.

He is currently with the Department of Psychology, University of Sheffield, Sheffield, U.K., where he is engaged in human and computer vision with J. Mayhew and J. Frisby and has a continuing interest in the psychophysics of human stereo vision. His research interests include video tracking of eye movements and building the EyeLab open-source model of the extraocular muscle system and computational models of the role of the cerebellum in the control of eye movements.